

Compressible dynamic stall vorticity flux control using a dynamic camber airfoil

M S CHANDRASEKHARA

Department of Mechanical and Astronautical Engineering, Naval Postgraduate School, Monterey, CA 93943, USA
e-mail: mchandra@nps.edu

Abstract. This study reports control of compressible dynamic stall through management of its unsteady vorticity using a variable droop leading edge (VDLE) airfoil. Through dynamic adaptation of the airfoil edge incidence, the formation of a dynamic stall vortex was virtually eliminated for Mach numbers of up to 0.4. Consequently, the leading edge vorticity flux was redistributed enabling retention of the dynamic lift. Of even greater importance was the fact that the drag and pitching moment coefficients were reduced by nearly 50%. The camber variations introduced when the leading edge was drooped are explained to be the source of this benefit. Analysis of the peak vorticity flux levels allowed the determination of minimum necessary airfoil adaptation schedule.

Keywords. Compressible dynamic stall; unsteady vorticity control; camber effects flow control.

1. Introduction

The potential for producing twice the lift by rapidly pitching an airfoil past the static stall angle than is achieved in steady flow, is the major reason for the keen interest in the phenomenon of dynamic stall. It has long been established that this benefit is due to the additional circulation associated with the leading edge dynamic stall vortex. However, its uncontrolled convection over the airfoil surface produces extremely violent pitching moment fluctuations that can even lead to structural failure of aircraft components. Thus, a wing or a rotor blade, and other systems, such as a wind turbine, are prevented from ever entering dynamic stall, essentially disregarding potential improvements in performance. As excessive demands are placed on future generations of such systems, an overwhelming need has developed to avail this benefit safely. The motivation for the present study stems from this goal.

In the dynamic stall problem, compressibility effects appear at a very low freestream Mach number of 0.2 (Carr 1988). The primary reason is the large flow-acceleration induced in the flow by rapid unsteadiness. The mechanisms of compressible dynamic stall onset have been discussed by Chandrasekhara *et al* (1998). Regardless of the onset mechanism, a dynamic stall vortex always forms. The preponderance of the dynamic stall vortex in the flow dictates that any control technique be devised to carefully manage the flow vorticity. Above a hitherto

unknown threshold level, the vorticity coalesces into a vortex whose behaviour cannot be controlled. However, the vorticity is needed to generate dynamic lift. Thus, a flow-control approach must diffuse the vorticity prior to its coalescence, but keep the vorticity over the airfoil up to the higher angles of attack. As vorticity is an intractable quantity, indirect methods are required to estimate its levels in the flow to establish the success of flow control. Reynolds & Carr (1985) offer a way towards this end by relating the vorticity flux at the surface (LHS) to the adverse pressure gradient as follows:

$$\nu \frac{\partial \Omega}{\partial n} = \frac{\partial U_s}{\partial t} + \frac{1}{\rho} \frac{\partial p}{\partial s} + V \Omega. \quad (1)$$

(Here s and n are coordinates along and normal to the airfoil surface, Ω is the vorticity, V is the surface mass transpiration velocity, U_s is the airfoil surface velocity, ρ is fluid density, ν is viscosity, p is local surface static pressure and t is time.) The first term on the RHS of the above equation is the surface tangential acceleration, the second, the potential flow pressure gradient, and the last, the surface transpiration, which is 0 in the present experiments where no suction or blowing was used. Reynolds & Carr (1985) also state that the first term is responsible for the generation of vorticity in the Stokes layer, which then diffuses outwards across the boundary layer. Now, the large amplitude unsteady motion of the surface induces a similar movement of the stagnation point, from which the flow accelerates as it negotiates the airfoil leading edge curvature. The vorticity flowing through the boundary layer can then be thought of as arising from the rapidly changing strong pressure gradient near the leading edge due to its unsteady motion. Thus, even though the vorticity is produced by the unsteady surface motion, it appears that its subsequent convection through the boundary layer over the airfoil upper surface can only be managed through the pressure gradient term, if it can be changed. Thus, the most significant flow control lever available is the pressure gradient term. Interestingly, it can be shown that the surface acceleration term is about one order smaller than the pressure gradient term for the dynamic stall conditions encountered by a helicopter-rotor retreating blade. Thus, only changes to the potential flow appear to offer the most potential for success, which inevitably requires geometry changes. Consequently, shape adaptation was explored for dynamic stall control here.

This paper discusses control of compressible dynamic stall using the novel idea of variable droop leading edge (VDLE) airfoil. The leading 25% of this airfoil was maintained at zero-degree incidence and the trailing 75% was oscillated sinusoidally over an angle of attack range $\alpha = 10^\circ + 10^\circ \sin \omega t$. The flow over the airfoil was documented with surface-mounted, unsteady, fast response, pressure transducers. Lift, drag and pitching moment coefficients were calculated from the pressure data. The measured pressures were also used to compute the vorticity flux distributions, which were later analyzed. From these, it became possible to deduce the minimum droop variations that could prove effective.

2. Experimental description

The experiments were conducted in the Compressible Dynamic Stall Facility (CDSF) (figure 1) at the NASA Ames Research Center. The tunnel can produce flow conditions appropriate for a helicopter retreating blade. Mach numbers of up to 0.55 are possible and, with an oscillating drive located on top of the test section, reduced frequencies ($k = \pi f c / U_\infty$, with f = airfoil oscillation frequency, c = airfoil chord and U_∞ = freestream velocity) of up to 0.2 can be realized.



Figure 1. A view of the compressible dynamic stall facility.

The VDLE airfoil was a 0.15 m chord VR-12 airfoil spanning the wind tunnel. It was made in two parts. The leading 25% of the airfoil was supported by a hinge-shaft at the quarter-chord point to produce various droop angles. The main element was attached to a hinge, which was held in the CDSF windows and oscillated synchronously with them. Twenty Kulite unsteady pressure transducers, at selected locations, provided the airfoil pressure distributions. The sensor electrical leads passed through the hollow hinge-shaft on the drooping front portion of the airfoil, which also protruded from the CDSF windows, figure 2. It was linked to drive arms on both sides of the test section. When the arms were anchored to the windows, a

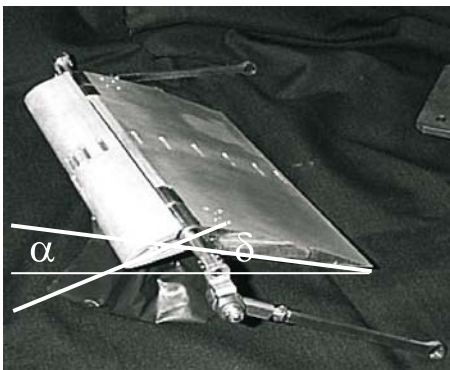


Figure 2. Assembled VDLE airfoil (Chandrasekhara *et al* 2004).

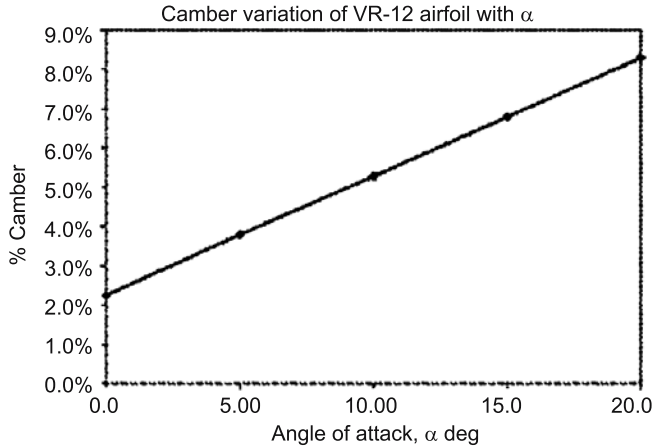


Figure 3. VR-12 camber variation with angle of attack.

fixed leading-edge droop angle resulted. On the other hand, if the arms were anchored to the stationary tunnel sidewalls, a sinusoidally varying leading edge droop was obtained. The resulting camber variation for the airfoil is shown in figure 3. The conditioned analog signals from the sensors were simultaneously acquired using a high-speed A-D converter along with a digital encoder signal that provided the airfoil instantaneous angle-of-attack information. Since absolute pressures were measured, considerable care was taken during calibration and experimentation to account for changes in ambient pressure (caused by weather), noise, drift and other such extraneous factors (Chandrashekhara *et al* 2004). The paper discusses data for the condition, droop $\delta =$ angle of attack, α (see figure 2 for the definitions of these angles). The performance parameters were computed from the measured data as explained earlier (Chandrashekhara *et al* 2004).

The data were phase-resolved prior to ensemble averaging. The pressure data were fitted with a cubic spline curve, and the airfoil surface was measured using a profilometer at a very high resolution. The pressure gradient distribution at each instantaneous angle of attack was then calculated from these curves to serve as the vorticity-flux distributions in accordance with (1). In all calculations, the surface acceleration term was neglected (Reynolds & Carr 1985).

3. Results and discussion

Figure 4 presents the lift coefficient ($C_l = 2(\text{lift})/c \cdot \rho U_\infty^2 / \text{unit span}$) distributions for the basic VR-12 airfoil (no leading edge droop, $\delta = 0^0$) and when it is operated in the VDLE mode for $M = 0.3$, $k = 0.1$. It is clear that in both cases, a large increase in lift is generated, when compared to the steady flow case also shown in the figure. Thus, dynamic stall benefit is retained in the VDLE mode (figure 4); even though the lift increment is slightly less, the angle at which the peak lift occurs differs. The lift distribution for the VR-12 airfoil indicates the formation of the dynamic stall vortex in the flow, as evidenced by the drop and a subsequent steep rise of C_l , whereas that for the VDLE airfoil shows only a slow decrease. This is one key difference pointing to achieving successful flow control.

Interestingly, the drag comparisons (not shown) revealed that the pressure drag was notably (about 50%) less for the VDLE airfoil at the post static stall angles of a VR-12 airfoil. Figure 5

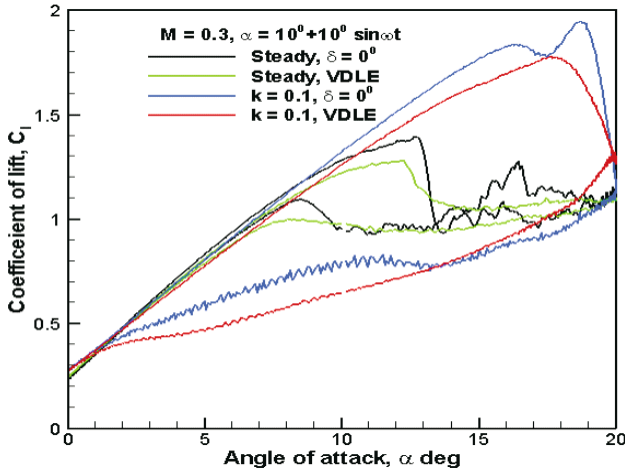


Figure 4. Life coefficient distributions, $M = 0.3$.

compares the pitching moment coefficient ($C_m = 2(\text{moment})/c^2 \cdot \rho U_\infty^2$) distributions for the unsteady cases of the two airfoil configurations. The basic VR-12 airfoil experiences a negative C_m distribution that becomes greatly exaggerated at $\alpha \approx 16^\circ$, which coincides with the beginning of the dynamic stall vortex convection (as determined from interferometry measurements). The C_m loop also crosses over (see arrows) and the net area under the curve indicates negative aerodynamic damping. In comparison, the VDLE case shows a gradual fall in C_m values towards the higher angles of attack, consistent with the increase in the airfoil camber. Furthermore, the loop does not cross-over and the area under it is negative, pointing to positive aerodynamic damping.

An even more dramatic difference is seen at $M = 0.4$, as shown in figures 6 and 7 where the measured pressure coefficient ($c_p = 2(p - p_\infty)/\rho U_\infty^2$) distributions are compared for the VR-12 and the VDLE airfoils respectively. The VR-12 airfoil produces large suction

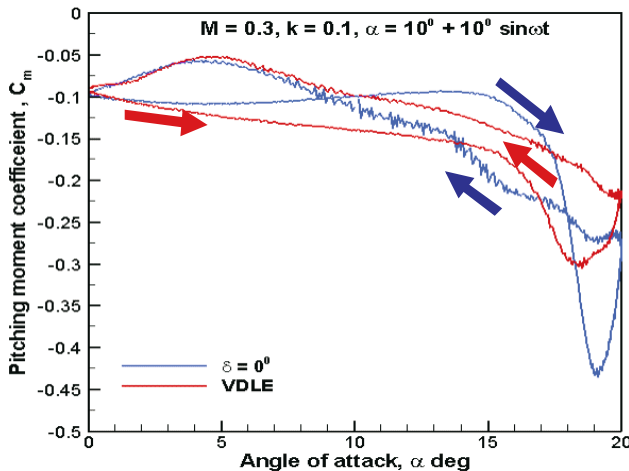


Figure 5. Pitching moment coefficient distributions, $M = 0.3$.

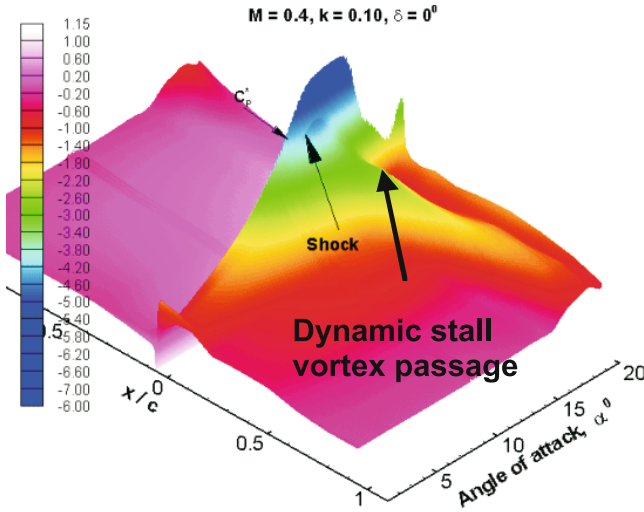


Figure 6. Surface pressure distributions, $M = 0.4, k = 0.1, \delta = 0^\circ$, VR-12 airfoil.

pressures and the local flow exceeds critical values (beginning of blue in the figures) over a large range of angles of attack. Shocks form in the flow, persist over a range of angles of attack (figure 6) and, eventually, dynamic stall vortex ensues from shock-induced separation and convects over the airfoil upper surface over about $1-1.5^\circ$ angle-of-attack further pitch-up of the airfoil as shown. The leading-edge suction remains at considerably high values even as this process progresses, almost contradicting the fact that the rest of the airfoil is dominated by stall with a large low pressure region, before it also drops. On the other hand, the pressure plot in figure 7 for the VDLE airfoil shows that dynamically varying the camber by leading-edge drooping has the effect of significantly reducing the leading-edge suction pressure. In fact, it does not even exceed the critical value. Thus, no shocks can form and dynamic stall originates as a pressure gradient driven event rather than shock-induced. The absence of a

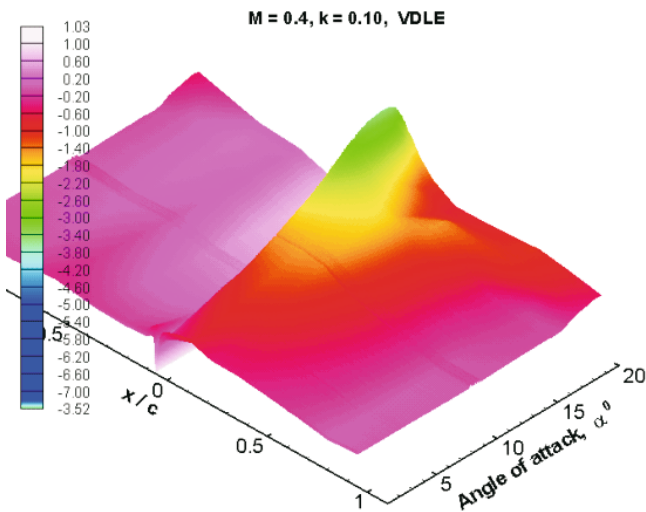


Figure 7. Surface pressure distributions, $M = 0.4, k = 0.1$, VDLE-airfoil.

sharp rise in the local surface pressure at the core of the convecting vortex, as it passes over the airfoil upper surface in figure 7 indicates that the vortex is much weaker. Thus, the entire airfoil unsteady stall behaviour is modified by dynamic drooping of the leading edge.

The above comparison confirms two major differences when the VR-12 airfoil is changed dynamically to a VDLE airfoil.

- (1) The dynamic stall phenomenon, in particular the concomitant vortex, is completely avoided at $M = 0.3$ and as a consequence, the VDLE airfoil yields a highly favorable pitching moment distribution.
- (2) The dynamic stall behaviour is completely modified at $M = 0.4$ and the type of stall-onset mechanism is changed from shock-induced to pressure-induced.

As stated in § 1, such dramatic changes can only be produced if the vorticity field is significantly altered. The following discussion addresses the physics of the problem considering the vorticity-flux distributions.

The vorticity flux was derived from curve fits from (1) as described earlier by curve-fitting the ensemble-averaged pressure distributions and taking the derivative from the surface contours measured at high resolution. The interest here is the peak level of the vorticity flux and the way it drops as the angle of attack is increased in both cases. It is recalled here that the control philosophy was that by reducing the peak vorticity flux level, the vortex formation process can be hindered and the flow can be kept attached and the dynamic lift sustained for beneficial use. Figure 8 shows the values at various angles over the entire upper surface at $M = 0.4$ and $k = 0.1$. As the flow accelerates with increasing angle of attack, the large suction developed eventually produces a shock at $\alpha \approx 11^\circ$. The shock persists over a range of airfoil angles of attack and gets stronger during further pitch-up of the airfoil. However, when the shock acquires adequate strength, separation ensues and the vortex is abruptly shed. The level of the vorticity flux appears to decrease because of the diffusion associated with the vortex and the vortex imprint is not as strong as was seen in figure 6. Owing to this reason, pressure data were used in figure 6 to establish its formation and passage. Still, the peak vorticity level is about 250 units (value obtained from processed data tables) prior to dynamic stall onset.

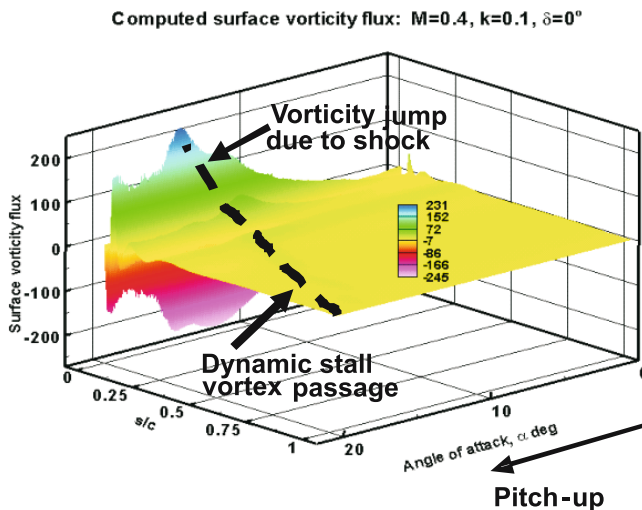


Figure 8. Computed vorticity-flux distributions, $M = 0.4, k = 0.1$, VR-12 airfoil.

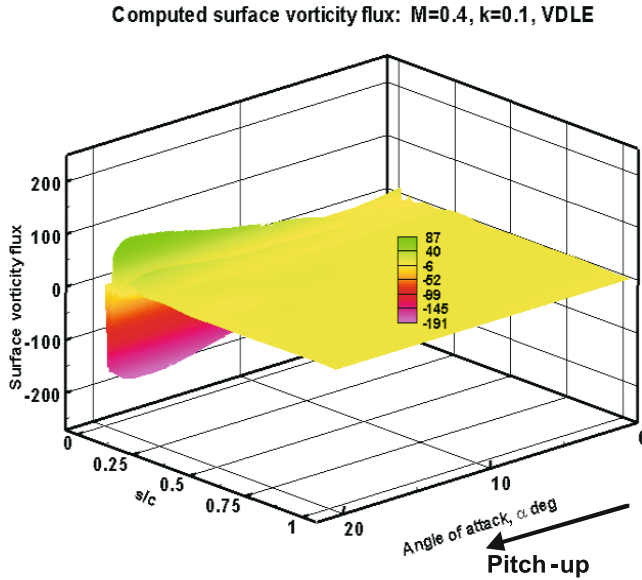


Figure 9. Computed vorticity-flux distributions, $M = 0.4$, $k = 0.1$, VDLE airfoil.

Now, if we consider figure 9, which shows the same data for the VDLE airfoil, it is very clear that the peak vorticity level has reached only a value of about 75–80 units over all the angles of attack of interest. Also, the distributions have become significantly broader and smoother. The peak vorticity value is attained near the end of the upstroke and it then falls gradually, lending support to the conclusion that dynamic stall, if at all present, is now a gradual process and its vortex is weak over the VDLE airfoil. The redistribution of the vorticity flux achieved in the process is clearly evident when figures 8 and 9 are compared. The obvious question from a practical standpoint is what the most optimum leading edge droop schedule would be that would produce the desired result while not placing undue demands on the actuators that are used for such an operation. Even on a model scale of 0.15 m, the lift produced by the leading edge section is large and in a full scale rotor it is likely to be about 50 times larger if the entire blade span was chosen for leading edge drooping. Thus, significant actuator loads may be encountered. The large amplitude of actuation used in these tests and its high frequency will need to be fine-tuned to suit such flight conditions. Figure 10 is drawn in an effort to establish some workable boundaries for the droop schedule.

Experiments were separately conducted for Mach numbers ranging from 0.2 to 0.4 and reduced frequencies of 0.05 and 0.1 for fixed droop cases of $\delta = 5, 10, 15$ and 20° for which the percentage camber is known. From each table of vorticity flux computed for the sinusoidal motion, the maximum value was chosen for plotting in figure 10. The dynamically varying camber cases of the VDLE airfoil are shown in figure 10 at an arbitrary value of 10% camber. Of greatest interest here is the near steep drop of the peak vorticity flux level over a small range of about 4% camber, generally between 3% and 7%. The rapid drop in the peak level suggests that a leading-edge droop schedule in which the airfoil can retain its basic shape until a certain angle of attack is reached on the upstroke, at which position its nose can be drooped over a small angle of attack range to produce a camber of around 6%, held there for the rest of the cycle and then returned to its basic shape at perhaps the same point on the downstroke. The potential advantage this could offer, in addition to placing a lesser demand on the actuator,

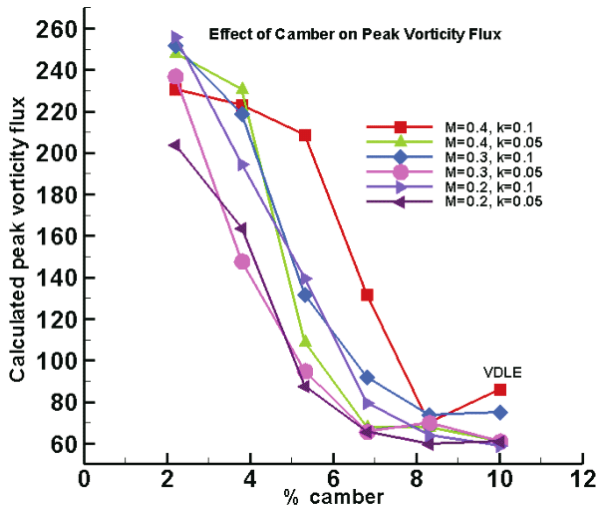


Figure 10. Variation of peak vorticity flux vs % camber of various flow conditions.

is that the lift coefficient which seemed to fall slightly as the angle of attack was increased may also be retained at a higher value for a longer portion of the cycle and in effect, improve the performance as well. Whereas this latter point still remains to be established, the results presented would provide some insight into the minimum extent of droop schedules that might produce desirable results.

Another unknown here is the rate of leading edge droop, but it is also a parameter whose effect is still to be studied. The time scale (degree of unsteadiness) at which this is carried out may be expected to have a bearing on the retention of the unsteady vorticity and its redistribution over the upper surface.

4. Conclusions

Study of compressible dynamic stall control has been conducted using the novel idea of a variable droop leading edge airfoil. The phenomenon was successfully controlled by the approach, and dynamic stall vortex was eliminated, along with its undesirable pitching moment variations at up to $M = 0.4$, $k = 0.1$. Analysis of the data showed that the process of control involved redistribution of the dynamic stall vorticity, such that the peak vorticity was always kept below the level that causes a dynamic stall vortex to form. When dynamic stall occurred, the flow control approach altered the phenomenon to a predominantly pressure gradient driven one, and the dynamic stall vortex was at best a mild structure. As a result, the lift coefficient was only about 10% lower than a basic VR-12 airfoil, but the drag and pitching moment coefficients were drastically decreased by as much as 50%. The present study used a drooping schedule $\delta = \alpha$, but the analysis led to the conclusion that a less demanding droop schedule can also be as successful.

The author acknowledges the support of US ARO and AFDD in the conduct of this study through the agencies' support to the Naval Postgraduate School.

References

- Carr L W 1988 Progress in analysis and prediction of dynamic stall. *AIAA J. Aircr.* 25: 1–25.
- Chandrasekhara M S, Wilder M C, Carr L W 1998 Competing mechanisms of compressible dynamic stall. *AIAA J.* 36: 387–393
- Chandrasekhara M S, Martin P B, Tung C 2004 Compressible dynamic stall control using a variable droop leading edge airfoil. *AIAA J. Aircr.* (41): 862–869
- Reynolds W C, Carr L W 1985 Review of unsteady, driven, separated flows. AIAA Paper No. 85-0527